Four-dimensional magnetic resonance imaging (4D-MRI) using image-based respiratory surrogate: A feasibility study

Jing Cai,[a] Zheng Chang, and Zhiheng Wang
Department of Radiation Oncology, Duke University Medical Center, Durham, North Carolina 27710

William Paul Segars
Department of Radiology, Duke University Medical Center, Durham, North Carolina 27710

Fang-Fang Yin
Department of Radiation Oncology, Duke University Medical Center, Durham, North Carolina 27710

(Received 8 July 2011; revised 12 October 2011; accepted for publication 18 October 2011; published 9 November 2011)

Purpose: Four-dimensional computed tomography (4D-CT) has been widely used in radiation therapy to assess patient-specific breathing motion for determining individual safety margins. However, it has two major drawbacks: low soft-tissue contrast and an excessive imaging dose to the patient. This research aimed to develop a clinically feasible four-dimensional magnetic resonance imaging (4D-MRI) technique to overcome these limitations.
Methods: The proposed 4D-MRI technique was achieved by continuously acquiring axial images throughout the breathing cycle using fast 2D cine-MR imaging, and then retrospectively sorting the images by respiratory phase. The key component of the technique was the use of body area (BA) of the axial MR images as an internal respiratory surrogate to extract the breathing signal. The validation of the BA surrogate was performed using 4D-CT images of 12 cancer patients by comparing the respiratory phases determined using the BA method to those determined clinically using the Real-time position management (RPM) system. The feasibility of the 4D-MRI technique was tested on a dynamic motion phantom, the 4D extended Cardiac Torso (XCAT) digital phantom, and two healthy human subjects.
Results: Respiratory phases determined from the BA matched closely to those determined from the RPM: mean (±SD) difference in phase: −3.9% (±6.4%); mean (±SD) absolute difference in phase: 10.40% (±3.3%); mean (±SD) correlation coefficient: 0.93 (±0.04). In the motion phantom study, 4D-MRI clearly showed the sinusoidal motion of the phantom; image artifacts observed were minimal to none. Motion trajectories measured from 4D-MRI and 2D cine-MRI (used as a reference) matched excellently: the mean (±SD) absolute difference in motion amplitude: −0.3 (±0.5) mm. In the 4D-XCAT phantom study, the simulated "4D-MRI" images showed good consistency with the original 4D-XCAT phantom images. The motion trajectory of the hypothesized "tumor" matched excellently between the two, with a mean (±SD) absolute difference in motion amplitude of 0.5 (±0.4) mm. 4D-MRI was able to reveal the respiratory motion of internal organs in both human subjects; superior–inferior (SI) maximum motion of the left kidney of Subject #1 and the diaphragm of Subject #2 measured from 4D-MRI was 0.88 and 1.32 cm, respectively.
Conclusions: Preliminary results of our study demonstrated the feasibility of a novel retrospective 4D-MRI technique that uses body area as a respiratory surrogate. © *2011 American Association of Physicists in Medicine*. [DOI: 10.1118/1.3658737]

Key words: 4D-MRI, 4D-CT, tumor motion, respiratory motion, cine-MRI

I. INTRODUCTION

Four-dimensional computed tomography (4D-CT) has been widely used in radiation therapy to assess patient-specific breathing motion for determining individual safety margins.[1–5] However, 4D-CT involves high imaging dose to the patient due to increased scan time,[6–8] and does not provide sufficient information about soft-tissue respiratory motion due to low soft-tissue contrast. Conversely, MRI has excellent soft-tissue contrast and imposes no radiation hazard. An MRI-based 4D imaging technique, namely 4D-MRI, is therefore highly desirable in the radiation therapy (RT) clinic.

At present, there is no established 4D-MRI technique for RT. Several methods have been proposed,[9–14] yet none have been implemented in the clinic due to either insufficient image quality or excessive technical involvement. Two main approaches have been taken in 4D-MRI development: (1) to use fast 3D MR sequences to acquire real-time volumetric images (i.e., real-time 4D-MRI), and (2) to use fast 2D MR sequences to continuously acquire images from all respiratory phases and then retrospectively sort these images by respiratory phase (i.e., retrospective 4D-MRI). The first approach is typically accomplished with parallel imaging and echo sharing techniques. However, limitations of

currently available hardware and software make it impossible to acquire high resolution 4D image sets without significantly compromising image quality. Typical temporal resolution of real-time 4D-MRI is greater than 1 s and typical voxel size is approximately 4 mm. This temporal resolution is inadequate compared to a typical human's breathing cycle of 4–5 s. For example, Dinkel *et al*. used a 3D time-resolved echo shared gradient echo technique combining parallel imaging with view sharing (TREAT) sequence to demonstrate how the individual motion pattern of lung tumors may vary in patients with diaphragmatic palsy.[9] The temporal resolution was 1.4 s and the voxel size was $3.1 \times 3.1 \times 4$ mm in this study. Blackall *et al*. implemented a dynamic 3D MRI technique using fast file echo with echo planar imaging (FFE-EPI).[10] They achieved an acquisition of 330 ms/frame but the image quality was insufficient to show structures in detail. Overall, the image quality of real-time 4D-MRI is low due to the lack of spatial resolution and to motion artifacts blurring fast-moving structures. The loss of image quality can be partially compensated for by co-registration with high quality reference images.

The second approach requires some form of respiratory surrogate (internal or external) to monitor patient motion during image acquisition. Compared to real-time 4D-MRI, the image quality is improved: motion artifacts are largely reduced due to fast image acquisition, and voxel size is smaller with increased in-plane spatial resolution. Remmert *et al*. demonstrated a retrospective 4D-MRI technique on a dynamic lung phantom using an external signal for motion monitoring.[11] The pixel size was 2.7×2.7 mm at 10 mm slice thickness. The external signal was derived from the positional changes of the piston rod of the water pump, which is obviously inappropriate for use with human subjects. Von Siebenthal *et al*. developed a retrospective 4D-MRI technique using a navigator slice at a fixed position for motion monitoring.[12] All images were acquired in sagittal planes and an alternating scheme was used to acquire data frames at all slice positions interleaved with navigator frames, with an in-plane resolution of 1.8×1.8 mm and out-of-plane resolution of 3–4 mm. Disadvantages of this technique include the need for sequence modification and longer acquisition time as every other image is acquired purely for sorting purposes.

In addition to the two approaches described above, a unique adaptive 4D-MRI technique was developed by Tokuda *et al*. using navigator echoes and multiple gating windows.[13] The navigator echo technique was used to monitor the respiratory signal in real-time during a scan. The respiratory signal is segmented into several bins/gating windows, and each *k*-space is filled with MR echo data acquired in the associated bin. The complex nature of this technique is the major factor limiting its implementation in radiation therapy.

The current research aims to develop a robust, reliable, and clinically practical 4D-MRI technique. To achieve both technical simplicity and sufficient image quality, we developed a retrospective 4D-MRI technique that uses standard 2D cine MR sequence for image acquisition, eliminating the requirement for sophisticated MR pulse sequence development. In addition, we extracted respiratory signals directly from the images, using the body area (BA) as respiratory surrogate, eliminating the need for external motion monitoring devices. The accuracy of 4D-MRI for motion measurement was assessed using phantoms and the feasibility of 4D-MRI on human subjects was explored.

II. METHODS AND MATERIALS

II.A. Validation of BA as a respiratory surrogate

The rationale for using BA as a respiratory surrogate is based on the fact the that human body expands and contracts during the breathing. To evaluate BA as a respiratory surrogate, we performed a validation study on 12 cancer patients (6 female, 6 male, mean age 64.1), including 6 lung cancer patients and 6 abdominal cancer patients. The study was carried out using the patients' presorted 4D-CT images and the corresponding Real-time Position Management (RPM) data. These 4D-CT images were acquired on a GE four-slice CT scanner (Lightspeed Plus 4, GE Healthcare, Waukesha, WI), along with the RPM system (Varian Medical Systems, Inc., Palo Alto, CA) and ADVANTAGE4D software (GE Healthcare, Milwaukee, WI). A plastic box with a pair of reflective markers was placed on the patient's anterior abdominal surface. The scanner was operated in axial cine mode, with continuous scans performed at each couch position with an interval equal to 1–1.5 s plus the patient's average respiratory period. Data acquisition was repeated at each couch position until full longitudinal coverage of the region of interest was obtained. Imaging parameters were: 120 kV, 2.5-mm slice thickness, gantry rotation of 0.5 s, matrix resolution of 512×512.

Figure 1 shows the workflow of how to extract breathing signals from presorted 4D-CT images using the BA method. Firstly, each CT image was processed by applying a threshold of −350 Hounsfield units to determine the body contour. Morphological operations were then performed to exclude extraneous pixels in the image that were above the threshold due to noise. BA was defined as the number of pixels within the body contour [white area in Fig. 1(b)]. In practice, the BA was calculated using only the central part of the CT image [grey area in Fig. 1(b)] where the respiratory-induced movement is most significant. Secondly, an individual breathing curve [Fig. 1(c)] was generated at each slice location by plotting the BA as a function of image acquisition time. The mean of the BA values was set to zero. Since our CT scanner images four slices simultaneously, the breathing curve for a couch position was the average of the four breathing curves for the four slices. Finally, the complete breathing curve [Fig. 1(d)] was generated by putting together all individual breathing curves according to the image acquisition time. Since the 4D-CT image acquisition stops during couch movements (approximately 2.3 s) between consecutive couch positions, there are gaps between the individual breathing curves.

Respiratory phases were calculated in a systematic approach due to the existence of gaps in the complete breathing signals: (1) peak(s) and valley(s) were detected for each

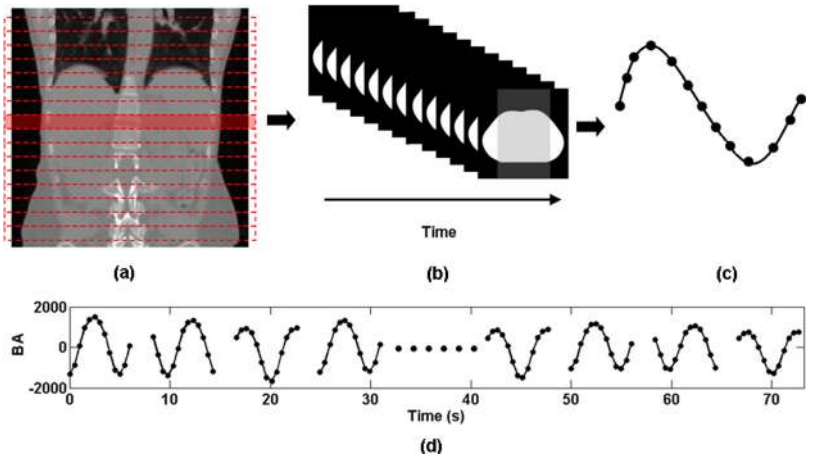

FIG. 1. Workflow of extracting breathing signals from presorted 4D-CT images using the BA method. (a) 4D-CT images were acquired in axial planes; each slice was imaged continuously throughout the breathing cycle. (b) BA (white area) was determined for each image. In practice, only the middle section of the image (grey area) was used for BA calculation. (c) For each image slice, an individual breathing curve was generated by plotting the BA as a function of image acquisition time. (d) The completed breathing signal is generated by plotting all individual breathing curves as a function of acquisition time. Gaps between individual breathing curves are due to couch movements during the 4D-CT scans.

individual breathing curve (neither peak nor valley can be the first or the last data point); (2) if the individual breathing curve had at least two peaks/valleys, a breathing period was calculated as the time period between the two peaks/valleys (Ideally this should be the case for all individual breathing curves due to the sufficient data requirement of 4D-CT; however, in reality this is not always true due to patients' breathing irregularity); (3) an average breathing period was determined as the mean of the breathing periods determined in step 2, followed by the determination of an average bin size (assuming 10 bins in one breathing cycle); (4) respiratory phases were calculated separately for each individual breathing curve in different scenarios: if there were at least two peaks/valleys, the peaks/valleys were set to Phase 50%/0%, and the phases for other data points were calculated via linear interpolation; if there was only one peak and/or one valley, the peak/valley was set to Phase 50%/0%, and the phases for other data points were calculated based on the average bin size determined in step 3.

To evaluate the performance of the BA as a respiratory surrogate, we compared the BA-derived phases to the RPM-derived phases, which were used as the gold-standard. Prior to the comparison the RPM-derived phases were: (1) rescaled from the range of 0–2π to the range of 0%–100% to match the scale of the BA-derived phases, and (2) undersampled to keep only the data points at the image acquisition times. (Note that RPM data acquisition rate is 30 data points per second, while CT image acquisition rate is approximately 3 frames per second). The following parameters were calculated from the comparison for each patient: correlation coefficient (r), mean phase difference (d), and mean absolute phase differences ($|d|$).

II.B. 4D-MRI technique

Our 4D-MRI technique was achieved by employing a fast 2D MR sequence to acquire axial images continuously throughout the breathing cycle, and then retrospectively sorting the MR images based on the respiratory phases. The MR sequence used for image acquisition was a fast steady state acquisition imaging technique (labeled as FIESTA by GE and TrueFISP by Siemens). It was chosen due to its high temporal resolution (up to 6–8 frames/s) and good tumor visibility. This sequence has been widely used for real-time tumor motion imaging.[14–18] MRI parameters were optimized to balance signal-to-noise ratio (SNR), spatial resolution (~1.5 mm in-plane pixel size), and temporal resolution (~3 frames/s).

Respiratory signals and phases were determined using a similar process as described in Sec. II A. There were two major differences. (1) The threshold used to determine the body contour was different. For MR images, the threshold was around 50 and can vary slightly between patients. We found that a good patient-specific threshold can be estimated as the image noise multiplied by a factor of 3. (2) There were no gaps in the complete breathing curve of the 4D-MRI since there was no couch movement during MR image acquisition. In this case, the complete breathing curve was obtained by plotting individual breathing curves continuously without zeroing their means. The variation of the complete breathing curve was mainly caused by two factors: respiration and anatomic change (for example, body size increases from neck to thorax). As we are only interested in respiration-induced changes, the second factor was unwanted and therefore was removed from the breathing curve. This was accomplished by firstly applying a low-pass filter to generate a "base body area curve" and then subtracting it from the complete "body area curve." The resulted breathing curve, named as "rescaled body area curve," was then used for respiratory phase determination. Since there were no gaps in the breathing curve, respiratory phases were directly calculated by first assigning all the peaks to Phase 50% and then calculating the rest via linear interpolation. Finally, MR images were retrospectively sorted according to respiratory phase. In the case where a phase was missing, the nearest adjacent phase (and the corresponding MR image) was used for 4D-MRI reconstruction. All image processing and data analysis were performed using an in-house program implemented in MATLAB (The MathWorks Inc., Natick, MA), which allowed for manual correction for errors in automatic peak detection.

II.C. Motion phantom study

A phantom apparatus was constructed in-house, consisting of a MRI-compatible motion stage and a motion motor

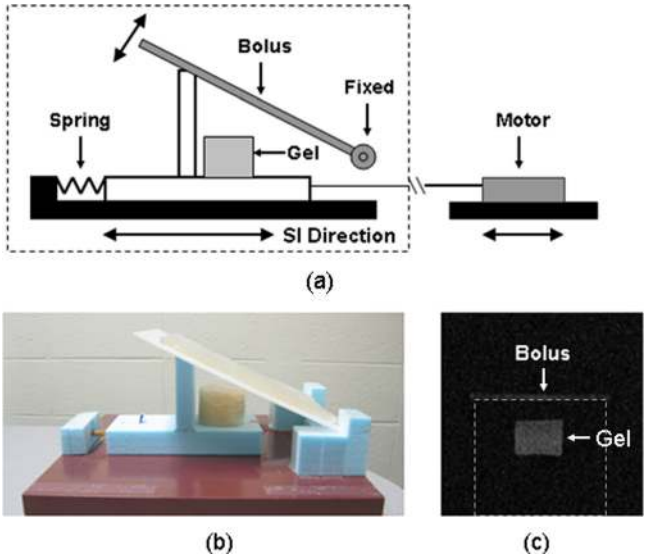

FIG. 2. (a) Sketch of the phantom design, and (b) the real phantom (motor is not shown). During the MRI experiment, objects within the dashed line were placed inside of the MR scanner, and the motion motor was placed outside the MR scanner. (c) Axial MR image of the phantom showing the determination of the BA (dashed box).

(BrainLAB Inc., Feldkirchen, Germany). The sketch of the phantom apparatus and the real phantom are shown in Fig. 2. The motion stage consists of a supporting platform (2 cm solid water slab), an inverse-T shaped motion stage made from styrofoam, a cylindrical imaging object made from gel (radius = 2.3 cm, height = 3.2 cm), and a 5 mm-thick bolus piece on a plastic flat board. The motion stage was driven by a motor on one end via a surgical low-elastic thread and attached to the other end via a rubber band. During the MR experiments, the motion stage was placed in the MR scanner while the motor was placed approximately 3 m away from the center of the scanner. The motor was set to move in a sinusoidal wave (peak-to-peak amplitude = 2.0 cm, period = 5 s), driving the motion stage to move in the same pattern. Consequently, the imaging object moved along the superior–inferior (SI) direction, while the bolus piece rotated along the fixed axis, simulating the tumor motion and the body surface motion, respectively. Repeatability and accuracy of phantom motion has been previously verified.[19] (Note that due to the use of string and the added friction in the system, the phantom cannot perfectly reproduce the input motion trajectory. The actual motion of the phantom is therefore different from the input signal and was determined using the cine-MR images in this study.)

Four-dimensional-MRI of the phantom were performed on a clinical 1.5 T clinical scanner (Signa, GE Healthcare, Milwaukee, WI) using a FIESTA sequence and a six channel phased-array coil. Imaging parameters were: repetition time (TR)/echo time (TE), 3.2 ms/1.0 ms; field of view (FOV), 300×300 mm; flip angle, 50°; slice thickness, 5 mm; matrix, 192×128. Frame rate was ~3 frames/s. All images were acquired in axial planes; each slice was imaged for 6 s. The MR images were interpolated to 256×256 before further analysis. BA of the phantom was defined as the area under the bolus piece, as indicated by the dashed box in Fig. 2(c). Four-dimensional-MRI was reconstructed as described earlier. The phantom was also imaged in the sagittal plane across the center of the imaging object using 2D cine-MRI technique, which used the same MR sequence (FIESTA) as used in 4D-MRI and the same imaging parameters (except for single slice vs. multiple slices). Since cine-MRI acquires near real-time images, it was used to obtain the true motion of the phantom in the SI direction. The motion trajectory of the phantom determined from the cine-MRI served as a ground-truth, and was compared with that determined from the 4D-MRI.

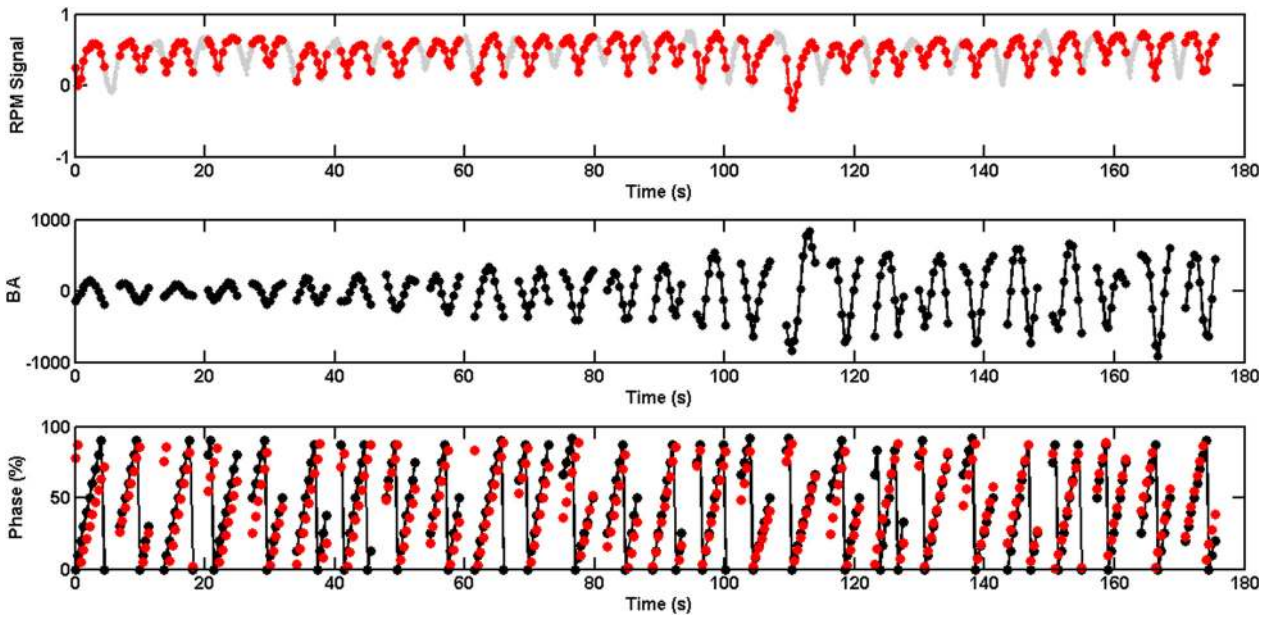

FIG. 3. Breathing signals and respiratory phases determine based on the BA surrogate, compared to those determined from the RPM system for a liver cancer patient.

TABLE I. Summary of patients' characteristics and measurements.

Patients	Age	Gender	Cancer site	Correlation coefficient (r)	Mean absolute phase difference ($|d|$)	Mean phase difference (d)
1	65	M	Lung	0.96	9.0	7.7
2	72	M	Lung	0.87	16.8	−14.2
3	60	M	Lung	0.95	7.9	−3.2
4	66	M	Lung	0.94	12.0	−9.9
5	70	F	Lung	0.98	12.8	−12.6
6	58	F	Lung	0.88	14.1	−9.1
7	72	F	Abdomen	0.96	5.9	1.2
8	38	M	Abdomen	0.97	5.5	−0.7
9	61	M	Abdomen	0.91	9.8	−1.3
10	67	F	Abdomen	0.90	9.9	−2.1
11	82	F	Abdomen	0.92	9.1	0.3
12	58	F	Abdomen	0.88	11.9	−2.9
Mean (±SD)	64.1 (±10.8)	/	/	0.93 (±0.04)	10.4 (±3.3)	−3.9 (±6.4)

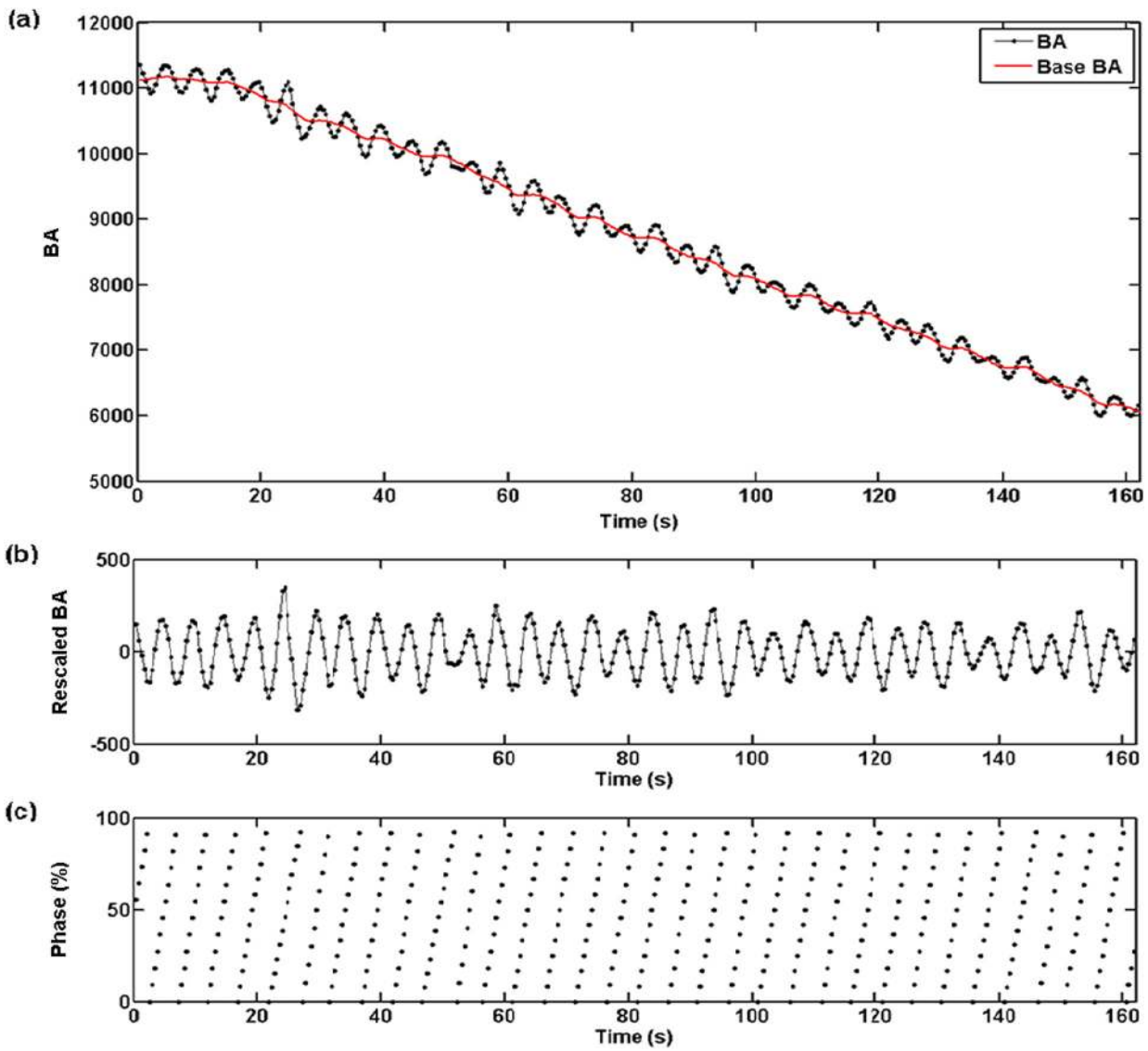

FIG. 4. Body area curve (a), rescaled body area curve (b), and respiratory phases (c) measured using the BA method for the phantom study.

II.D. 4D-XCAT Phantom study

We further validated the 4D-MRI technique using the 4D extended Cardiac Torso (XCAT) digital phantom developed by Segars *et al.*[20–22] Details about the XCAT phantom can be found in the literature and will not be repeated here. In summary, the 4D-XCAT phantom provides detailed and realistic anatomical structures and physiological functions suitable for use in higher-resolution imaging applications. It is capable of depicting the complex shapes of real human organs and the deformations of those shapes due to anatomical variation and normal physiological motion. The respiratory motion of the 4D-XCAT phantom was modeled using 4D respiratory gated CT from a normal human subject.

In this study the 4D-XCAT phantom was generated in the abdomen region with the following parameters: 256×256 in-plane resolution, 2 mm in-plane pixel size, 2 mm slice thickness, maximum diaphragm motion: 3.0 cm; maximum surface motion: 1.0 cm; breathing period: 5 s; frames per breathing cycle: 10. Default breathing curves were applied. The phantom was generated in the activity mode and the signal intensities of the anatomic tissues were assigned based on typical FIESTA/TrueFISP MR images of the abdomen.[23] A hypothesized spherical "tumor" of 3 cm in diameter was generated in the liver.

The 4D-MRI was simulated based on the 4D-XCAT in the following steps: (1) mimic the image acquisition by continuously extracting images of the same axial slice from the 4D-XCAT phantom for more than one breathing cycle; (2) repeat step 1 for all axial slices; (3) calculate the BA for each extracted axial slice and determine the breathing curve as described in the previous section; (4) calculate the respiratory phase for each extracted axial slice; and 5) retrospectively sort the extracted axial slices based on respiratory phase to generate the simulated "4D-MRI." Motion trajectories of the hypothesized "tumor" were determined from the simulated 4D-MRI and compared to those measured from the 4D-XCAT.

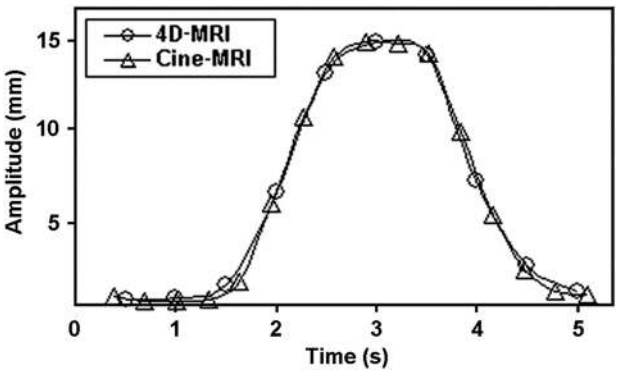

FIG. 6. Comparison of the motion trajectories of the imaging object determined from the sagittal 4D-MRI and the sagittal cine-MRI.

II.E. Human study

The feasibility of the 4D-MRI was tested on two healthy subjects, in the abdomen (Subject #1) and the thorax (Subject #2), respectively. The study was approved by Institutional Review Board and informed consent was obtained from each subject before the study. (The MR scans were performed at the University of Virginia. This study retrospectively analyzed the data.) MR images were acquired on a Siemens 1.5 T clinical scanner (Magnetom Avanto, Siemens Medical Solution, Germany) using a TrueFISP sequence and a four-element phased-array body coil and a spinal coil. The subjects were positioned head-first-supine with arms down and were instructed to breathe normally during the scans. No immobilization device was used. All MR images were acquired in axial planes, and each slice was imaged for a time equal to the subject's breathing period plus 1 s. Imaging parameters were: TR/TE, 3.7 ms/1.21 ms; FOV, 350×227 mm; flip angle, 52°; slice thickness, 5 mm; matrix, 256×166; bandwidth, 1300 Hz/pixel. Breathing signals were derived using the BA method as described above. Respiratory phases were calculated and 4D-MRI were reconstructed via retrospective sorting by phase.

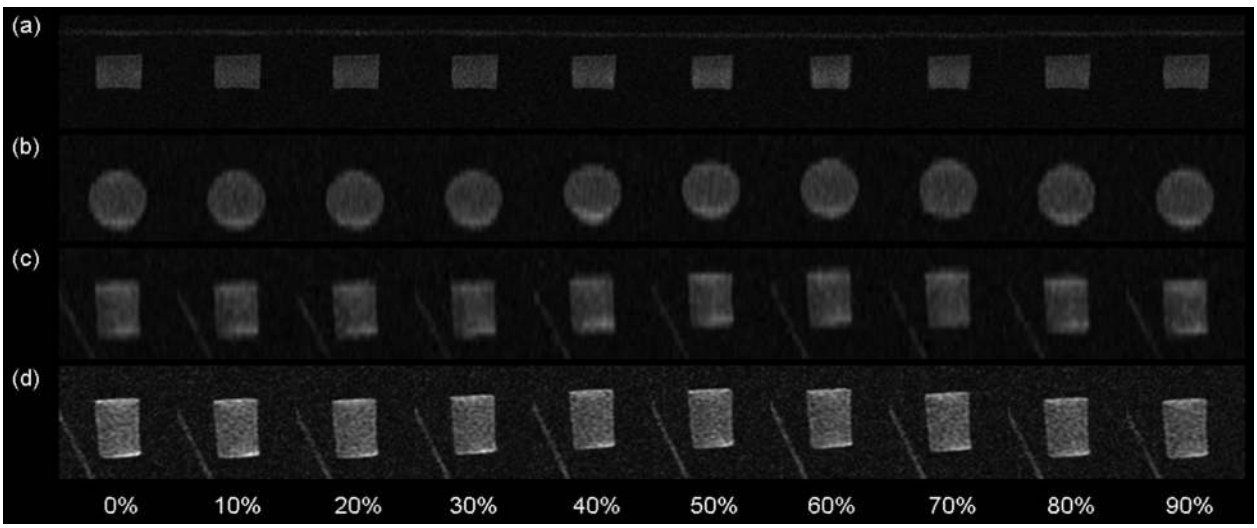

FIG. 5. Axial (a), coronal (b), and sagittal (c) 4D-MRI images, and sagittal cine-MRI images (d) of the imaging object.

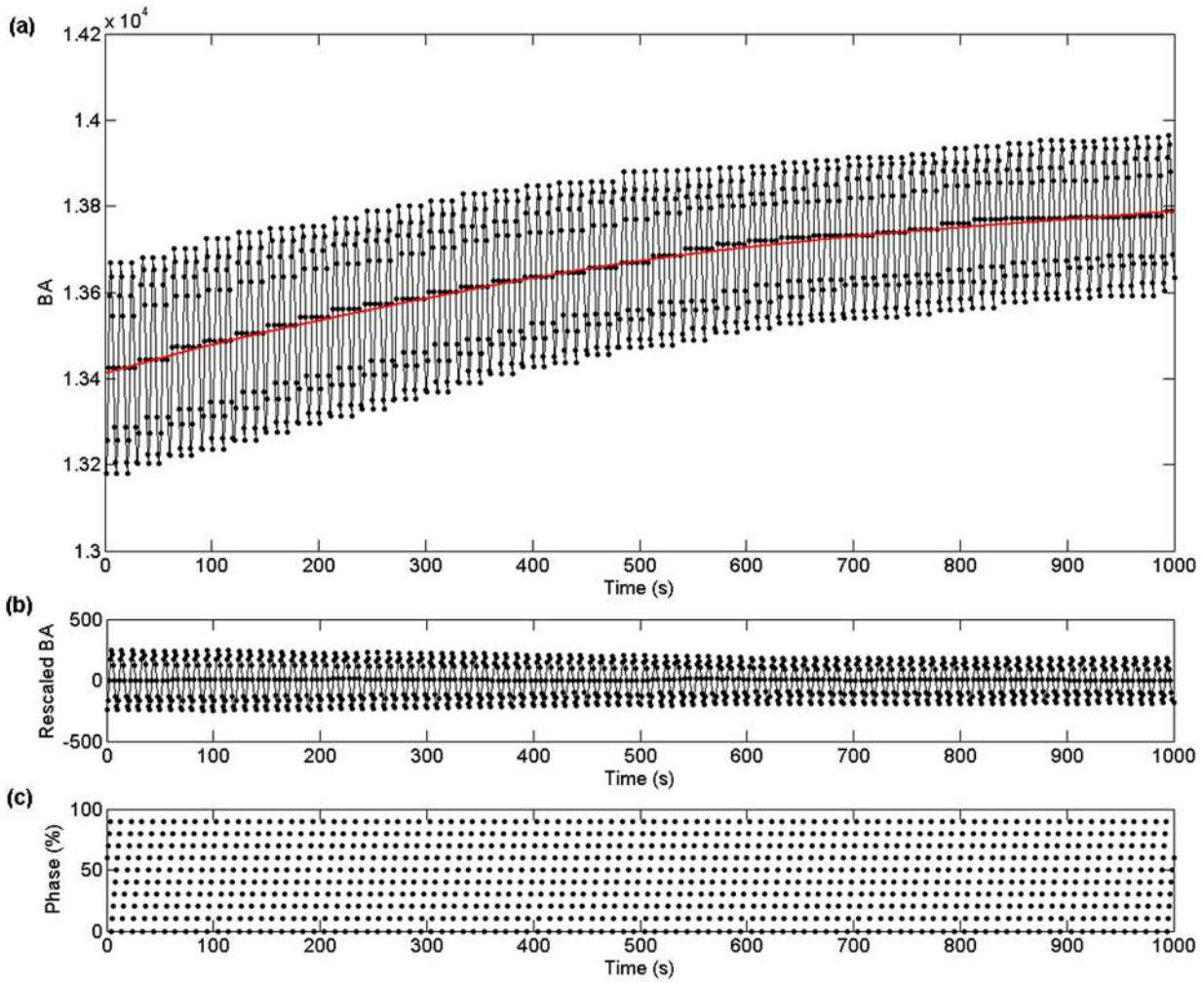

FIG. 7. Body area curve (a), rescaled body area curve (b), and respiratory phases (c) measured using the BA method for the 4D-XCAT phantom study.

III. RESULTS

III.A. Validation study

Figure 3 shows an example of the breathing signals and respiratory phases determined using the BA method, compared to those obtained from the RPM for a liver cancer patient. Despite the patient's apparent breathing irregularity as seen in the RPM signal, the respiratory phases determined from the two methods matched well (mean phase difference = 1.2%, mean absolute phase difference = 5.9%, and mean correlation coefficient = 0.96). On average for all 12 patients: mean phase difference was $-3.9 \pm 6.4\%$, mean absolute phase difference was $10.40 \pm 3.3\%$, and mean correlation coefficient was 0.93 ± 0.04. Table I summarizes the measurements.

III.B. Motion phantom study

Figure 4 shows the "breathing" signals and respiratory phases of the phantom determined using the BA method. The "base body area" decreased from the higher to the lower bolus position (refer to Fig. 2 for phantom design). The "rescaled body area" [Fig. 4(b)] shows the pattern of periodic motion (average period = 4.96 ± 0.30 s) that is consistent with the input signal. Small variations in the motion amplitude in the breathing signals was present but did not significantly affect peak detection and phase calculation. 4D-MRI images of the phantom, as shown in Fig. 5, clearly illustrated the motion of the imaging object in all three planes. Minimal image artifacts were observed, such as

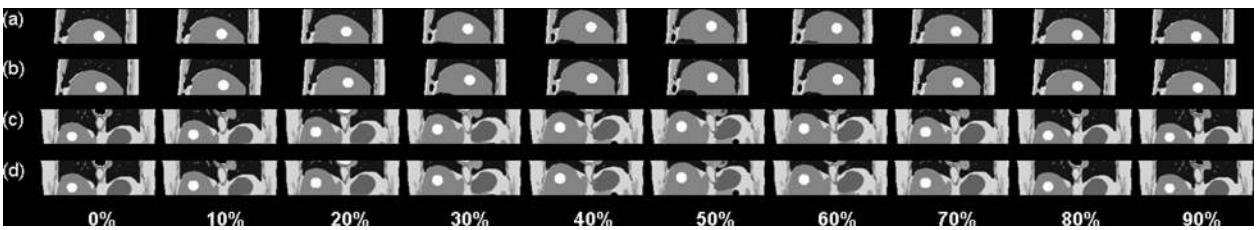

FIG. 8. Sagittal (a) and coronal (c) XCAT images compared to the sagittal (b) and coronal (d) images of simulated 4D-MRI.

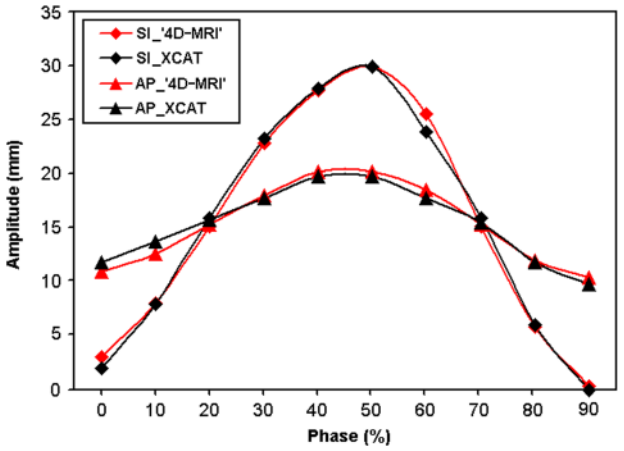

FIG. 9. Comparison of the motion trajectories of the hypothesized tumor determined from the simulated 4D-MRI and from the original 4D-XCAT phantom.

discontinuity between consecutive slices and interpolation-derived image blurring in the coronal and sagittal image. The overall image quality, however, was barely affected by the image artifacts. The motion trajectory of the imaged object measured from the sagittal 4D-MRI images [Fig. 5(c)] matched excellently with that measured from the cine-MRI images [Fig. 5(d)]. The mean absolute difference [±standard deviation (SD)] in motion amplitude between the two was − 0.3 (±0.5) mm, as shown in Fig. 6.

III.C. 4D-XCAT Phantom study

Figure 7 shows the breathing signals and respiratory phases of the 4D-XCAT phantom determined using the BA method. The simulated 4D-MRI images of the 4D-XCAT phantom, as shown in Fig. 8, showed good consistency with the original 4D-XCAT phantom images, in both sagittal and coronal planes. The motion trajectory of the hypothesized tumor also matched excellently in both SI and anterior–posterior (AP) directions between the two, as shown in Fig. 9, with a mean absolute difference (±SD) in motion amplitude of 0.5 (±0.4) mm.

III.D. Human study

Representative 4D-MRI images of Subjects #1 and #2 are shown in Figs. 10 and 11, respectively. Breathing signals and respiratory phases for Subject #1 are shown in Fig. 12 as an example. The "base body area" varied due to the subjects' anatomy changes [Fig. 12(a)]. The "rescaled body area" better illustrated the periodic breathing pattern of the subjects [Fig. 12(b)]. Image quality was degraded to a certain extent due to image artifacts such as discontinuities and inhomogeneous signal intensity, but was still adequate enough to reveal the respiratory motion of internal organs. For example, the motion of the kidneys in Subject #1 and the diaphragm in Subject #2 were clearly seen in the 4D-MRI images. Figure 13 show the motion trajectories of the left kidney of Subject #1 and of the diaphragm of Subject #2 that were determined from 4D-MRI images; the maximum motion in the SI direction was 0.88 and 1.32 cm, respectively.

IV. DISCUSSION

In this study we reported a retrospective 4D-MRI technique that uses BA as a respiratory surrogate. The preliminary results demonstrated that BA is a comparable respiratory surrogate to the RPM system and that the 4D-MRI technique can be used to image organ respiratory motion in both the thorax and the abdomen. However, further improvement in image quality of the 4D-MRI is desirable and will be the topic of our future research. It could be partly achieved via hardware upgrade (such as coil) and software enhancement (such as MR sequence optimization and further development of data analysis). While achieving simplicity by using BA as an internal respiratory surrogate, our 4D-MRI technique maintained similar spatial and temporal resolutions as other retrospective 4D-MRI techniques.

Although these preliminary results demonstrated that BA can be a good respiratory surrogate for 4D-MRI, further investigation on a larger pool of patients is still needed in order to answer the following questions: (1) Are there any differences between lung cancer patients and abdominal cancer patients when using BA as the respiratory surrogate? (2) How does breathing irregularity, patient weight, scan range, etc., affect the accuracy of respiratory phase measurements using the BA method? (3) Is the BA a better surrogate than external surrogates, in terms of correlation with internal tumor motion?

Image artifacts of 4D-MRI in this study stem mainly from two sources: MR imaging acquisition and retrospective sorting. It is well known that the FIESTA/TrueFISP sequences are normally affected by dark phase dispersion bands due to local field inhomogeneity.[14] Other image artifacts, such as

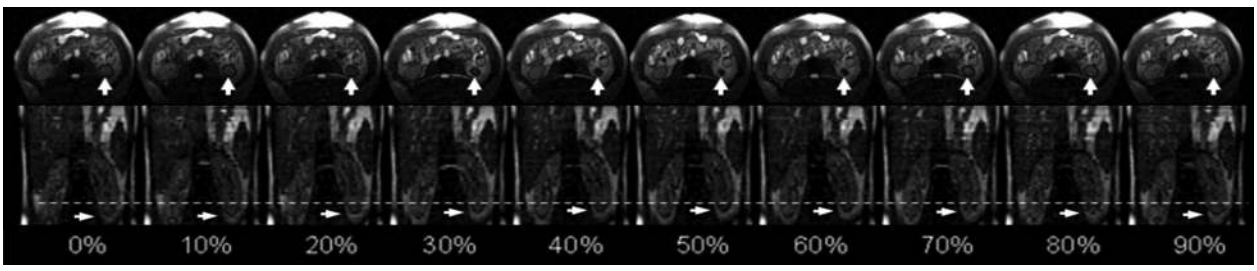

FIG. 10. Representative 4D-MRI images of Subject #1. Dash lines are drawn to facilitate the visualization of the respiratory motion. Arrows indicate the tracking point (inferior portion of the left kidney) that was selected to generate the motion trajectory.

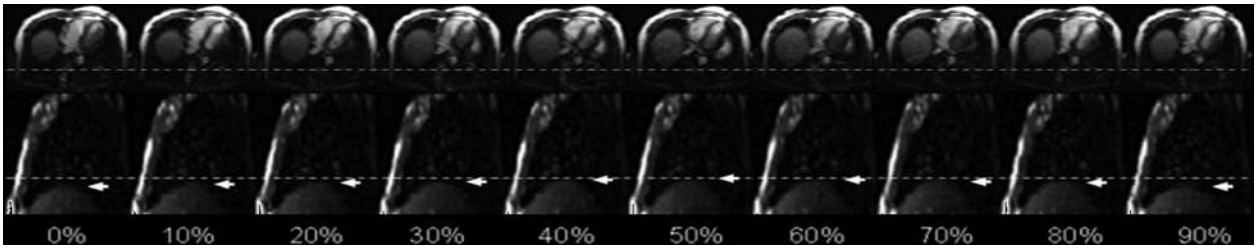

FIG. 11. Representative 4D-MRI images of Subject #2. Dash lines are drawn to facilitate the visualization of the respiratory motion. Arrows indicate the tracking point (diaphragm) that was selected to generate the motion trajectory.

ghost artifacts, may also appear in the MR images acquired using FIESTA/TrueFISP sequence. If these artifacts overlay regions of interest (ROIs) such as tumor or surrounding healthy tissues, it can cause errors in the delineation of these structures. In addition, MRI is known to have geometric distortion and various artifacts that are related to B_0 inhomogeneity and gradient nonlinearity. Correction algorithms provided by the vendors are often used to minimize the distortion errors, as we have done in our study. However, studies[24,25] have shown that the correction algorithms can only

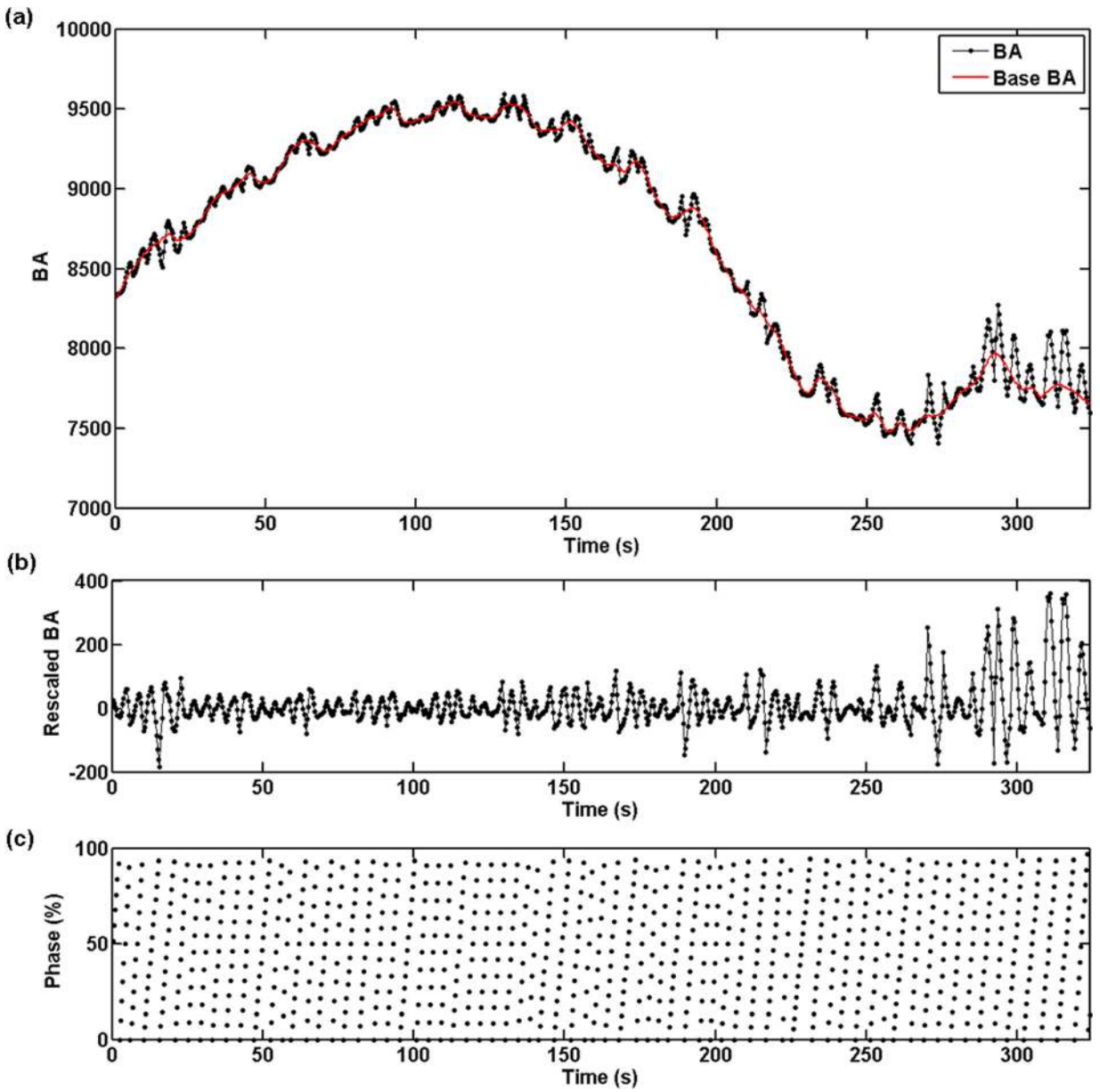

FIG. 12. Body area curve (a), rescaled body are curve (b), and respiratory phases (c) measured using the BA method for Subject #1.

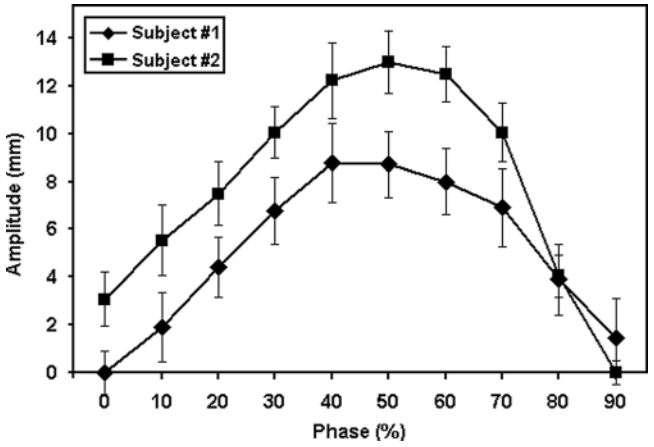

FIG. 13. Motion trajectories of the diaphragm of Subject #1 (diamonds) and of the left kidney of Subject #2 (rectangles) determined from the 4D-MRI. Standard deviations of multiple measurements were plotted as error bars.

correct in 2D, not in 3D. To completely eliminate the distortion error, a step and shoot technique has been introduced[25] and showed promising results of removing geometric distortions in 3D. We plan to incorporate this correction technique in our 4D-MRI technique in future research. Image artifacts related to retrospective sorting are caused by errors in respiratory phase calculation and by breathing irregularities.[3,4,15] These image artifacts typically present as tissue discontinuities in the reformatted coronal or sagittal images. Recognizing the common characteristics and understanding the causes of these image artifacts are critical in 4D-MRI applications, in order to minimize their adverse effects.

MR images were acquired in the axial plane in the current study. However, MR images can also be acquired in the sagittal plane, since the body area in sagittal images also varies with the patient's breathing. We chose the axial plane for two reasons: (1) 4D-CT acquires images in the axial plane. By keeping this convention, our 4D-MRI technique holds a greater similarity to the more familiar 4D-CT technique, potentially making its implementation in the clinic more straightforward; (2) respiratory motion in lateral body regions may be too small to be detected if images were acquired in the sagittal planes. It will be difficult, if not impossible, to extract breathing signals from these far-lateral sagittal images. Nevertheless, imaging in the sagittal plane has the advantage of encompassing the most significant motion information in the SI direction and minimal out-of-plane motion. It is of great interest to test the feasibility of imaging in the sagittal plane in future studies.

The 4D-MRI technique can be further improved in a number of ways. The accuracy of phase determination can be improved by using more sophisticated image processing and signal processing techniques such as wavelet analysis. The image quality can be enhanced by using a higher field MRI scanner and more advanced phased-array coils. 3T clinical MR scanners are now widely used and have been shown to effectively facilitate higher SNR/CNR, and higher spatial and/or temporal resolution than previously possible with MRI.[26,27] This study used a four-element phased-array coil, but state-of-the-art array coil systems include the use of up to 32 coils. Together with parallel imaging techniques such as sensitive encoding (SENSE), it can significantly boost the SNR and increase the temporal resolution. In addition, using audio/video couching to minimize patients' breathing variations may also potentially improve the accuracy of the BA surrogate, and subsequently the image quality of 4D-MRI.

There are several limitations in this study. Firstly, a single threshold was used to determine the BA contour. However, the MRI signal and noise often vary between patients and sometimes may even vary for the same patient. Using a single threshold to determine BA contour for all patients is suboptimal, if not impossible. In the next step of our research, we plan to implement an automatic determination of the threshold based on the background noise. The ultimate goal is to automatically and individually determine the optimal threshold for each series of MR images. Secondly, the effects of artifacts and noise on the accuracy of the motion measurements were not investigated in this study. However, considering that the main features of the MR images depend upon the sequence that is used, we expect the effects to be small. It is of interest to us to quantify such effects in our future studies. Thirdly, the number of human subjects was limited and there was no cancer patient data. The accuracy and robustness of the technique therefore needs further assessment in a later trial with a larger pool of human subjects. This is currently being investigated.

V. CONCLUSION

In this study, we demonstrated the feasibility of a novel retrospective 4D-MRI technique that uses body area as a respiratory surrogate on a dynamic motion phantom and healthy human subjects. Compared to other 4D-MRI techniques, this technique has the advantage of simplicity by eliminating the requirement for MR pulse sequence programming and external motion monitoring devices.

ACKNOWLEDGMENTS

The authors thank Dr. John P. Mugler III of the University of Virginia, who championed support for this study. We thank Drs. Yu Yuan and Shiva Das for providing the gel imaging object, and Dr. Jennifer O'Daniel for editing the manuscript. There is no conflict of interest involved in the work.

[a]Author to whom correspondence should be addressed. Electronic mail: jing.cai@duke.edu. Telephone: 919-684-1089; Fax: 919-660-2180.

[1]P. Keall, "4-dimensional computed tomography imaging and treatment planning," Semin. Radiat. Oncol. **14**, 81–90 (2004).
[2]D. A. Low *et al.* "A method for the reconstruction of four-dimensional synchronized CT scans acquired during free breathing," Med. Phys. **30**, 1254–1263 (2003).
[3]G. S. Mageras *et al.* "Measurement of lung tumor motion using respiration-correlated CT," Int. J. Radiat. Oncol., Biol., Phys. **60**, 933–941 (2004).
[4]T. Pan, "Comparison of helical and cine acquisitions for 4D-CT imaging with multislice CT," Med. Phys. **32**, 627–634 (2005).
[5]E. Rietzel, T. Pan, and T. Y. Chen, "Four-dimensional computed tomography: Image formation and clinical protocol," Med. Phys. **32**, 874–889 (2005).

[6]P. Keall *et al*. "Acquiring 4D thoracic CT scans using a multislice helical method," Phys. Med. Biol. **49**, 2053–2067 (2004).
[7]M. J. Murphy *et al*. "The management of imaging dose during image-guided radiotherapy: report of the AAPM Task Group 75," Med. Phys. **34**, 4041–4063 (2007).
[8]J. de Koste *et al*., "Renal mobility during uncoached quiet respiration: An analysis of 4DCT scans," Int. J. Radiat. Oncol. Biol. Phys. **64**, 799–803 (2006).
[9]J. Dinkel *et al*. "4D-MRI analysis of lung tumor motion in patients with hemidiaphragmatic paralysis," Radither. Onocl. **91**, 449–454 (2009).
[10]J. M. Blackall *et al*. "MRI-based measurements of respiratory motion variability and assessment of imaging strategies for radiotherapy planning," Phys. Med. Biol. **51**, 4147–4169 (2006).
[11]G. Remmert *et al*. "Four-dimensional magnetic resonance imaging for the determination of tumour movement and its evaluation using a dynamic porcine lung phantom," Phys. Med. Biol. **52**, N401–N415 (2007).
[12] M. Von Siebenthal *et al*. "4D MR imaging of respiratory organ motion and its variability," Phys. Med. Biol. **52**, 1547–1564 (2007).
[13]J. Tokuda *et al*. "Adaptive 4D MR imaging using navigator-based respiratory signal for MRI-guided therapy," Magn. Reson. Med. **59**, 1051–1061 (2008).
[14]C. Plathow *et al*. "Analysis of intrathoracic tumor mobility during whole breathing cycle by dynamic MRI," Int. J. Radiat. Oncol., Biol., Phys. **59**, 952–959 (2004).
[15]J. Cai *et al*. "Evaluation of the reproducibility of lung motion probability distribution function (PDF) using dynamic MRI," Phys. Med. Biol. **52**, 365–373 (2007).
[16]S. Shimizu *et al*. "High-speed magnetic resonance imaging for four-dimensional treatment planning of conformal radiotherapy of moving body tumors," Int. J. Radiat. Oncol., Biol., Phys. **48**, 471–474 (2000).
[17]H. U. Kauczor and C. Plathow, "Imaging tumour motion for radiotherapy planning using MRI," Cancer Imaging **31**, S140–S144 (2006).
[18]P. Bhosale, J. Ma, and H. Choi, "Utility of the FIESTA Pulse Sequence in Body Oncologic Imaging: Review," Am. J. Roentgenol. **192**, S83–S93 (2009).
[19]Z. Chang *et al*. "Evaluating dynamic magnetic resonance imaging using a new design of phantom: validation with fast megavoltage fluoroscopic imaging," Proceedings of AAPM 52nd Annual Meeting, Philadelphia PA, (2010).
[20]W. P. Segars *et al*. "4D XCAT phantom for multimodality imaging research," Med. Phys. **37**, 4902–4915 (2010).
[21]W. P. Segars *et al*. "MCAT to XCAT: The Evolution of 4-D Computerised Phantoms for Imaging Research," Proc. IEEE **97**, 1954–1968 (2009).
[22]W. P. Segars *et al*. "Realistic CT simulation using the 4D XCAT phantom," Med Phys, **35**, 3800–3808 (2008).
[23]R. Song *et al*. "Evaluation of respiratory liver and kidney movements for MRI navigator gating," J. Magn. Reson Imaging **33**, 143–148 (2011).
[24]D. Wang *et al*. "A novel phantom and method for comprehensive 3-dimensional measurement and correction of geometric distortion in magnetic resonance imaging," Magn. Reson. Imaging **22**, 529–542 (2004).
[25]E. S. Paulson *et al*. ""Step and Shoot MRI:" a Simple Acquisition Method to Reduce Gradient Nonlinearity-Induced Geometric Distortions for Radiation Treatment Planning," Med. Phys. **38**, 3770 (2011).
[26]M. C. DeLano *et al*. "Abdominal MR imaging at 3T," Magn. Reson. Imaging Clin. N. Am. **14**, 17–26 (2006).
[27]B. J. Soher *et al*., "A review of MR physics: 3T versus 1.5T," Magn. Reson. Imaging Clin. N. Am. **15**, 277–290 (2007).